Chemical Engineering Journal Advances 14 (2023) 100464

Contents lists available at ScienceDirect

Chemical Engineering Journal Advances

journal homepage: www.sciencedirect.com/journal/chemical-engineering-journal-advances

An analytical solution of the effectiveness factor of photocatalytic reactors based on Robin boundary conditions

Makiwe A. Nkohla [a,*], Buntu Godongwana [a], Veruscha G. Fester [b], Oluwafemi J. Caleb [c]

[a] Cape Peninsula University of Technology, Department of Chemical Engineering, PO Box 1906, Bellville, Cape Town, 7535, South Africa
[b] Cape Peninsula University of Technology, Faculty of Engineering & the Built Environment, PO Box 1906, Bellville, Cape Town, 7535, South Africa
[c] Africa Institute for Postharvest Technology, Faculty of AgricSciences, Stellenboch University, Private Bag X1, Stellenbosch, Stellenbosch, 7602, South Africa

ARTICLE INFO

Keywords:
Photocatalysis
Effectiveness factor
Robin boundary condition
Mathematical modelling
Sherwood number
Thiele modulus

ABSTRACT

An analytical expression of the effectiveness factor of photocatalytic reactors that accounts for external mass transfer limitations is presented. The solution is based on Robin boundary conditions introducing the Sherwood number as the parameter that accounts for the external mass transfer limitations. Regions highlighting free diffusion, diffusion limitations, and external mass transfer limitations are identified based on the Thiele Modulus and the Sherwood number. At low values of the Sherwood number, the internal diffusion and reaction rate-limiting regions are surpassed by the external mass transfer limitations. A cut-off value of the Sherwood number below which external mass transfer limitations cannot be ignored is 0.55. The evaluation of the model showed that under Dirichlet boundary condition the model converges to literature models from similar studies. This 1-D model looked at the Sherwood number across a broad scope and accounted for a broader range of limitations associated with immobilized photocatalytic films.

1. Introduction

The accumulation of excessive amounts of ethylene, a naturally occurring plant hormone [1], in fruit storage is one of the reasons for the loss of produce in the fruit and vegetable industry. This is because the fruit quality deteriorates due to over-ripening, increased pathogen susceptibility, physiological disorders, and senescence caused by over-exposure to ethylene [2]. Methods for combatting ethylene during postharvest storage will not only ensure food security thereby reducing losses but also impact the environment due to reduced waste that would have been dumped in the landfills, polluting the soil as well as the air.

Photocatalytic oxidation (PCO) has been shown to have the ability to delaying the adverse effects of ethylene in the storage atmosphere of fruit produce [3–9]. The technique utilizes photocatalytic material, usually, titanium dioxide (TiO_2) to decompose ethylene and other volatile organic compounds (VOCs) to H_2O and CO_2 under ultraviolet illumination. In photocatalytic processes, the photocatalyst is deposited as a thin film on support materials such as glass, stainless steel sheets, fibres, and many other materials. One of the advantages of immobilizing TiO_2 photocatalyst is that it results in a porous catalyst layer, providing a larger surface area for the degradation of the pollutant [10]. However, this thin catalyst film is usually subjected to mass transfer as well as photon absorption limitations. A good indication of the extent to which mass and photon transport limitations affect the immobilized photocatalytic layer is given by the effectiveness factor [11].

The effectiveness factor is the ratio of the actual reaction rate to the theoretical reaction rate if the whole surface area of the catalyst is available to the bulk concentration of the pollutant [12]. A few models found in literature that evaluated this parameter in photocatalytic reactions have focused only on the internal effectiveness factor which considers diffusion inside the catalyst layer [13,14]. Edwards et al., [14] used the orthogonal collocation method to determine the effectiveness factor for photocatalytic reactions obeying zero order, first order, second order, and generalized Langmuir-Hinshelwood/ Hougen-Watson kinetics. In their analysis, the convective mass transfer has been neglected based on the assumption that the polluted mixtures are sufficiently dilute. Based on the conclusions by the authors, the models, and the plots of effectiveness factor vs. Thiele Modulus presented may be applicable in the design of photocatalytic reactors, to account for varying concentrations and photon-flux levels within the catalyst film, thus, excluding the concentration profiles through the external film layer. Camera-Roda & Santarelli, [13] used the numerical solution by control volume method to determine the effectiveness factor in their study to investigate the optimum photocatalytic film thickness. One of the boundary conditions employed in their mathematical model is that

* Corresponding author.
E-mail address: nkohlam@cput.ac.za (M.A. Nkohla).

https://doi.org/10.1016/j.ceja.2023.100464

Available online 1 February 2023

Nomenclature

x	Position at the catalyst surface, m
δ	Catalyst layer thickness, m
L	Macroscopic length of the catalyst support, m
C_{Ab}	Concentration of the gas pollutant in the bulk, mol/m^3
C_A	Concentration profile through the gas film layer, mol/m^3
C_{A0}	Inlet concentration of species entering the reactor, mol/m^3
r	Radius of pores within the TiO_2 film, m
D_{AB}	Diffusion coefficient of the gas pollutant, m^2/s
$\dot{r}_A$	Reaction rate per unit irradiated surface area of the photocatalyst, mol/m^{2}s
r_0	Ideal reaction rate, mol/m^{2}s
$\bar{r}$	Average pore radius throughout the length of the coated TiO_2 film, m
k_r	Reaction rate constant, s^{-1}m^{-2}W^{-1}
I	UV light intensity, Wm^{-2}nm^{-1}
I_v	Intensity of the UV light entering the catalyst layer, Wm^{-2}nm^{-1}
k	Convective mass transfer coefficient, m/s
μ	Light absorption coefficient for UV in the catalyst, m^{-1}
C	Concentration profile of the species
X	Catalyst layer thickness
Δ	Optical thickness
ϕ	Thiele modulus
C_b	The ratio of the bulk concentration to the inlet species concentration
Sh	Sherwood number
Re	Reynolds number
Sc	Schmidt number
η	Effectiveness factor

of fixed concentration at the fluid–film interface. An analytical solution was presented by Visan et al., [15] for immobilized photocatalytic microreactors. The model is said to include the transport of species in the flow channel that is governed by advection and diffusion, however, convection through the film layer is not explicit in the equation for the effectiveness factor. Other authors simply used the effectiveness factor equation available in most chemical reactor design textbooks [16,17] for a straight cylindrical pore. Dijkstra et al., [18] used the equation to evaluate internal diffusion limitations in the immobilized catalyst for the photocatalytic degradation of formic acid. Krivec et al., [19] used the equation to account for pore diffusional effects in the photocatalytic degradation of phenol in a fixed TiO_2 microreactor. Murshed et al., [20] adopted the effectiveness factor equation by Fogler [12] to evaluate the internal mass transfer effects on the photodegradation of Astrazon Orange G (AOG) dye in spherical ZnO photocatalyst. It is worth noting that these equations were developed for conventional reactors and may not apply to photocatalytic reactors as they do not consider the UV light intensity.

The major limitation of the available effectiveness factor models is that they are developed based on the Dirichlet boundary type condition [13–15]. In this boundary condition, an assumption is that the bulk pollutant concentration is the same as the concentration at the catalyst surface, or that there is no external mass transfer resistance. This is not always true because of the species concentration gradient through the film layer. If the external mass transfer rate is low, the concentration in the bulk fluid and that at the external catalyst surface are significantly different [21]. Thus, the external mass transfer limitations which incorporate convection and diffusion of species in the film layer should be taken into account. The main aim of this work was to develop an analytical solution for the effectiveness factor that accounts for the external mass transfer limitations. The model was developed from the well known diffusion equation and solved by using the Robin boundary type instead of the Dirichlet boundary type condition, introducing the Sherwood number as one of the operating parameters. Robin boundary condition is well established in conventional reactors not utilizing photons but it is rarely used in solving photocatalytic reactions. In this article the expressions for both diffusional and external resistances are combined in one equation, hence the introduction of the Sherwood number. Thus, the developed model can accommodate cases where either only diffusional or external or both resistances are present.

2. Model development

2.1. Model description and assumptions

The photocatalytic reactor to be modelled is a continuous flow reactor utilizing a thin film of TiO_2 photocatalyst immobilized onto a porous nonwoven vilene and ultraviolet (UV) light as a source of photons. The basis of the model is depicted in Fig. 1(b), where $x = 0$ represents the position (m) at the catalyst surface, $x = \delta$ is the catalyst layer thickness (m) and L is the macroscopic length of the catalyst support (m). C_{Ab} is the concentration of the gas pollutant in the bulk and C_A (mol/m^3) is the concentration profile through the gas film layer. Fig. 1(c) shows the pores within the TiO_2 film assumed to be straight cylindrical with radius r.

The model will be based on the following operating conditions and assumptions: (1) the flow is steady and one-dimensional in the x direction; (2) the system is isothermal; (3) the diffusion coefficient (D_{AB}) is constant; (4) the reaction follows pseudo first order kinetics; and (5) the light intensity can be modelled using Beer Lambert's law. The purpose of the model is to determine a mathematical solution for the concentration profile through the photocatalyst that incorporates the change in concentration through the gas film layer. This concentration profile is then incorporated into the equation for calculating the effectiveness factor.

2.2. Governing equations

The catalyst layer in Fig. 1(b) can be represented in rectangular coordinates as shown in Fig. 2.

The mass balance in the x direction is given by:

$$\frac{\mathrm{d}}{\mathrm{dt}}(\rho \Delta x \Delta y \Delta z) = \left(J_{A,x|x} - J_{A,x|x+\Delta x}\right)\Delta y \Delta z - r_A(\Delta x \Delta y \Delta z) \quad (1)$$

Where $J_{A,x}$ is the diffusion flux of species A. Applying the steady state flow assumption and dividing through by $\Delta x \Delta y \Delta z$ gives:

$$0 = \frac{\left(J_{A,x|x} - J_{A,x|x+\Delta x}\right)}{\Delta x} - r_A \quad (2)$$

The term $J_{A,x|x+\Delta x}$ can be written as:

$$J_{A,x|x+\Delta x} = J_{A,x|x} + \Delta x \frac{dJ_{A,x}}{dx} \quad (3)$$

The diffusion flux is given by Fick's law:

$$J_{A,x} = -D_{AB}\frac{dC_A}{dx} \quad (4)$$

Substituting Eqs. (3) and (4) into Eq. (2) gives:

$$D_{AB}\frac{d^2C_A}{dx^2} = r_A \quad (5)$$

The reaction rate, r_A, in Eq. (5) is based on the unit reaction volume. As depicted in Fig. 1(b), the reaction of interest is a heterogeneous gas-

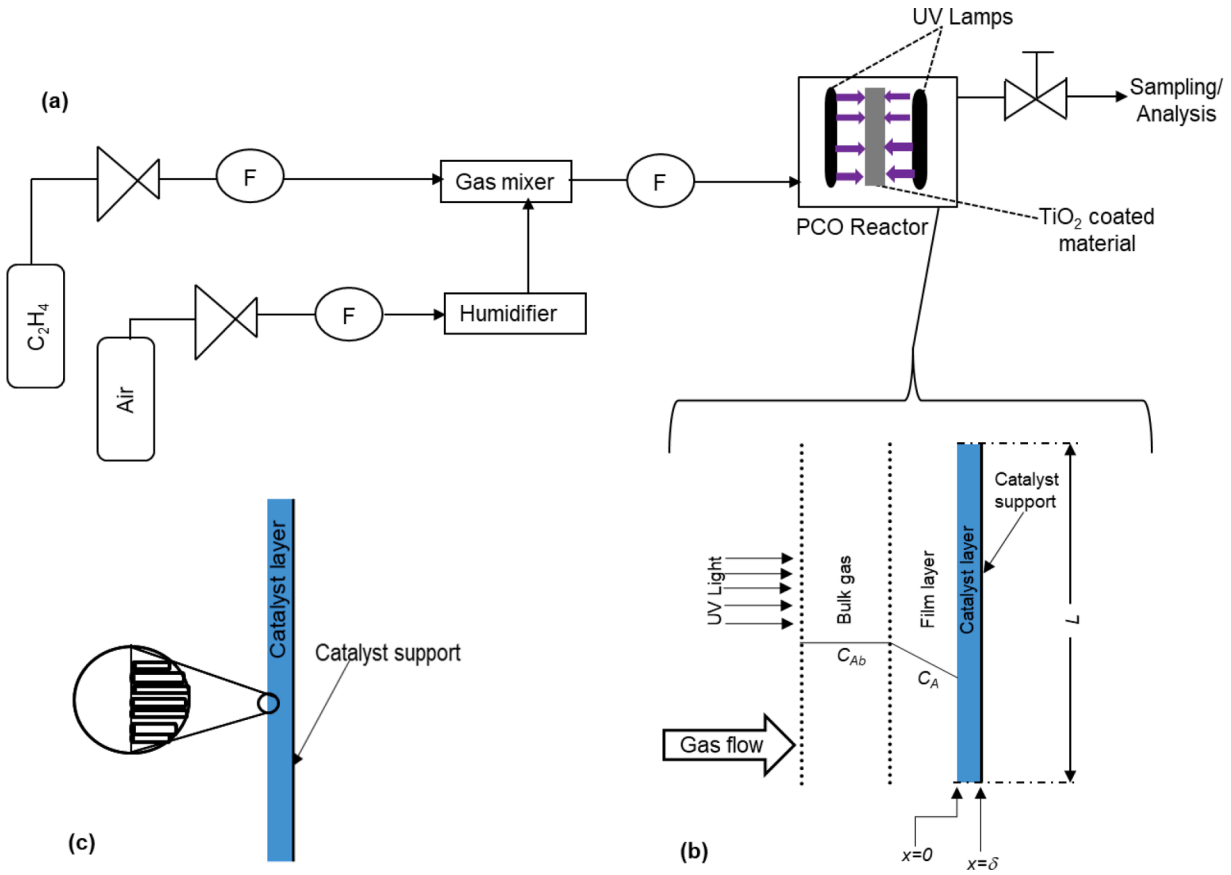

Fig. 1. Flow diagram of the photocatalytic reactor process (a) and the schematic of the concentration profile in the immobilized photocatalytic system (b); TiO_2 pores within the catalyst layer (c).

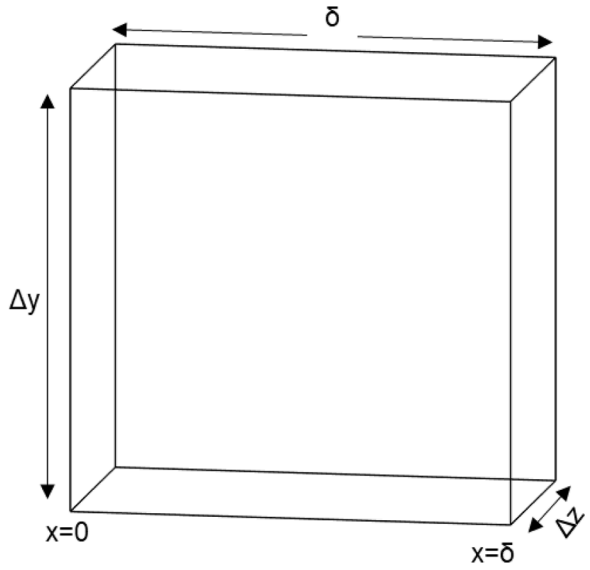

Fig. 2. Representation of the catalyst layer.

solid type which is dependent on the catalyst surface area. It is therefore necessary to redefine the reaction rate in terms of the unit surface area of the catalyst using the following relation:

$$\dot{r}_A A_s = r_A V_R \tag{6}$$

Where $A_s = 2Lz$ is the catalyst surface area, $V_R = Lz\bar{r}$ is the reaction volume and $\dot{r}_A$ is the reaction rate per unit irradiated surface area of the photocatalyst. Rearranging Eq. (6) and substituting the definitions of A_s and V_R gives:

$$r_A = \dot{r}_A\left(\frac{2Lz}{Lz\bar{r}}\right) = \dot{r}_A\left(\frac{2}{\bar{r}}\right) \tag{7}$$

Substituting Eq. (7) into Eq. (5) results in the diffusion-reaction equation:

$$D_{AB}\frac{d^2C_A}{dx^2} = \dot{r}_A\left(\frac{2}{\bar{r}}\right) \tag{8}$$

Eq. (8) may be nondimensionalized by introducing the dimensionless variables:

$$C = \frac{C_A}{C_{A0}};\ X = \frac{x}{\delta};\ R = \frac{\dot{r}_A}{r_0}$$

where r_0 is the reaction rate per unit area evaluated at the surface of the catalyst. Substituting the dimensionless variables into Eq. (8) and rearranging gives:

$$\frac{d^2C}{dX^2} = \left(\frac{2\delta^2}{C_{A0}D_{AB}\bar{r}}\right)\dot{r}_A \tag{9}$$

By further assuming that the efficiency of photons conversion to an oxidizing hole is constant, the reaction rate for ethylene PCO has been proven to be directly proportional to the light intensity [22]. Therefore, the reaction rate for reactions following the Langmuir-Hinshelwood (L-H) model can be written as:

$$\dot{r}_A = k_r I\frac{K_{ads}C_A}{1 + K_{ads}C_A} \tag{10}$$

Where k_r and I are the reaction rate constant and the UV light intensity

respectively. The Beer-Lambert law is widely used to model UV light intensity:

$$I = \mathrm{I_v}[\exp(-\mu x)] \tag{11}$$

Where I_v is the intensity of the UV light entering the catalyst layer and μ is the light absorption coefficient for UV in the catalyst. Combining Eqs. (9),(10), and (11), and applying dimensional analysis gives:

$$\frac{\mathrm{d^2C}}{\mathrm{dX^2}} = \left[\left(\frac{2\delta^2 \mathrm{I_v k_r}}{\mathrm{D_{AB}\bar{r}}}\right)\left(\frac{1}{\frac{1}{\mathrm{C_{A0}K_{ads}C}}+1}\right)\right]\exp(-\Delta \mathrm{X}) \tag{12}$$

where $\Delta = \mu\delta$ is the dimensionless optical thickness. For the first order approximation stated in the assumptions (i.e., if $1/C_{A0}K_{ads} >> 1$), the equation becomes:

$$\frac{\mathrm{d^2C}}{\mathrm{dX^2}} = \phi^2 \mathrm{C}[\exp(-\Delta \mathrm{X})] \tag{13}$$

where ϕ^2 is the Thiele modulus defined as:

$$\phi^2 = \frac{2\delta^2 \mathrm{I_v k_r}}{\mathrm{D_{AB}\bar{r}}} \tag{14}$$

Eq. (13) can be solved analytically by making use of the following transformation:

Let;

$$y = \exp(-\Delta \mathrm{X}) \tag{15}$$

Then;

$$\frac{\mathrm{dy}}{\mathrm{dX}} = -\Delta[\exp(-\Delta \mathrm{X})] \tag{16}$$

The derivativedC/dX in Eq. (13) may be written as:

$$\frac{\mathrm{dC}}{\mathrm{dX}} = \frac{\mathrm{dy}}{\mathrm{dX}}\frac{\mathrm{dC}}{\mathrm{dy}} = -\Delta[\exp(-\Delta \mathrm{X})]\frac{\mathrm{dC}}{\mathrm{dy}} \tag{17}$$

Therefore;

$$\frac{\mathrm{d^2C}}{\mathrm{dX^2}} = \Delta^2[\exp(-\Delta \mathrm{X})]\frac{\mathrm{dC}}{\mathrm{dy}} + \Delta^2[\exp(-2\Delta \mathrm{X})]\frac{\mathrm{d^2C}}{\mathrm{dy^2}} \tag{18}$$

Substituting Eq. (18) into Eq. (13) results in the following transformed form which is the modified Bessel equation:

$$\frac{\mathrm{d^2C}}{\mathrm{dy^2}} = -\frac{1}{\mathrm{y}}\frac{\mathrm{dC}}{\mathrm{dy}} + \left(\frac{\phi}{\Delta}\right)^2 \frac{1}{\mathrm{y}}\mathrm{C} \tag{19}$$

2.3. Solution of the model

The analytical solution to Eq. (19) is:

$$\mathrm{C} = \mathrm{C_1 I_0}\left(\frac{2\phi\sqrt{\mathrm{y}}}{\Delta}\right) + \mathrm{C_2 K_0}\left(\frac{2\phi\sqrt{\mathrm{y}}}{\Delta}\right) \tag{20}$$

Substituting the expression for y as defined by Eq. (15), the concentration profile is then given by:

$$\mathrm{C} = \mathrm{C_1 I_0}\left(\frac{2\phi\sqrt{\exp(-\Delta \mathrm{X})}}{\Delta}\right) + \mathrm{C_2 K_0}\left(\frac{2\phi\sqrt{\exp(-\Delta \mathrm{X})}}{\Delta}\right) \tag{21}$$

Where I_0 and K_0 are the zero order modified Bessel functions of the first and second kind respectively. The constants C_1 and C_2 may be determined by applying the following boundary conditions:

$$\mathrm{B.C.1 : at\ X = 0;}\quad \frac{\mathrm{dC}}{\mathrm{dX}} = -\mathrm{Sh}(\mathrm{C_b} - \mathrm{C}) \tag{22}$$

$$\mathrm{B.C.2 : at\ X = 1;}\quad \frac{\mathrm{dC}}{\mathrm{dX}} = 0 \tag{23}$$

Boundary condition 1 (B.C.1) is the Robin type boundary condition in which C_b is the ratio of the bulk concentration to the inlet species concentration and, *Sh* is the Sherwood number defined as:

$$\mathrm{Sh} = \frac{\mathrm{k}\delta}{\mathrm{D_{AB}}} \tag{24}$$

Where k is the convective mass transfer coefficient. The Sherwood number takes into account the diffusion resistance in the gas film layer. There are many mass transfer correlations in literature from which the Sherwood number can be calculated. Most studies in gas phase photocatalytic reactions have used the correlation (Eq. (25)) by [23]. A recent correlation (Eq. (26)) specifically for photocatalytic reactions using TiO_2 coated fibrous catalyst was developed by [24].

$$\mathrm{Sh} = 0.705\left(Re\frac{\mathrm{L}}{\delta}\right)^{0.43} Sc^{0.56} \tag{25}$$

$$\mathrm{Sh} = 0.0059 Re^{0.4663} Sc^{\frac{1}{3}} \tag{26}$$

where *Re* is the Reynolds number, and *Sc* is the Schmidt number. Applying the boundary conditions results in the following expressions for C_1 and C_2 respectively:

$$\mathrm{C_1} = \frac{\mathrm{ShC_b K_1}\left(\frac{2\phi}{\Delta}\sqrt{\exp(-\Delta)}\right)}{\mathrm{I_1}\left(\frac{2\phi}{\Delta}\sqrt{\exp(-\Delta)}\right)\left[\mathrm{ShK_0}\left(\frac{2\phi}{\Delta}\right) - \phi \mathrm{K_1}\left(\frac{2\phi}{\Delta}\right)\right] + \mathrm{K_1}\left(\frac{2\phi}{\Delta}\sqrt{\exp(-\Delta)}\right)\left[\mathrm{ShI_0}\left(\frac{2\phi}{\Delta}\right) + \phi \mathrm{I_1}\left(\frac{2\phi}{\Delta}\right)\right]} \tag{27}$$

$$\mathrm{C_2} = \frac{\mathrm{ShC_b I_1}\left(\frac{2\phi}{\Delta}\sqrt{\exp(-\Delta)}\right)}{\mathrm{I_1}\left(\frac{2\phi}{\Delta}\sqrt{\exp(-\Delta)}\right)\left[\mathrm{ShK_0}\left(\frac{2\phi}{\Delta}\right) - \phi \mathrm{K_1}\left(\frac{2\phi}{\Delta}\right)\right] + \mathrm{K_1}\left(\frac{2\phi}{\Delta}\sqrt{\exp(-\Delta)}\right)\left[\mathrm{ShI_0}\left(\frac{2\phi}{\Delta}\right) + \phi \mathrm{I_1}\left(\frac{2\phi}{\Delta}\right)\right]} \tag{28}$$

Table 1
Comparison of analytical and asymptotic solutions (Sh = 0.001, Δ = 0.1).

Thiele Modulus	Effectiveness Factor Analytical solution	Asymptotic solution
0.001	0.95072	0.98649
0.005	0.92951	0.97509
0.01	0.86891	0.90893
0.05	0.28156	0.28563
0.1	0.09046	0.09087
0.5	0.00398	0.00397
1	0.00099	0.00098
1.5	0.00044	0.00040
2	0.00025	0.00016

Where I_1 and K_1 are the first order modified Bessel functions of the first and second kind respectively.

The effectiveness factor, η may be defined as follows:

$$\eta = \frac{-D_{AB}\frac{dC_A}{dx}}{r_0} = \frac{-D_{AB}\frac{dC_A}{dx}}{k_r C_b I_v} \tag{29}$$

The reaction rate, r_0 is the ideal rate that would be obtained if the bulk concentration is maintained through the entire photocatalytic film and the incident photon flux does not attenuate through the film.

In dimensionless form Eq. (29) may be written as:

$$\eta = \frac{-1}{\phi^2}\frac{dC}{dX} \tag{30}$$

Combining Eqs. (21),27,(28), and (30) results in the following equation for the effectiveness factor:

$$\eta = \frac{1}{\phi}\frac{Sh C_b\left[K_1\left(\frac{2\phi}{\Delta}\sqrt{\exp(-\Delta)}\right)I_1\left(\frac{2\phi}{\Delta}\right) - I_1\left(\frac{2\phi}{\Delta}\sqrt{\exp(-\Delta)}\right)K_1\left(\frac{2\phi}{\Delta}\right)\right]}{I_1\left(\frac{2\phi}{\Delta}\sqrt{\exp(-\Delta)}\right)\left[Sh K_0\left(\frac{2\phi}{\Delta}\right) - \phi K_1\left(\frac{2\phi}{\Delta}\right)\right] + K_1\left(\frac{2\phi}{\Delta}\sqrt{\exp(-\Delta)}\right)\left[Sh I_0\left(\frac{2\phi}{\Delta}\right) + \phi I_1\left(\frac{2\phi}{\Delta}\right)\right]} \tag{31}$$

For a quick estimation of the effectiveness factor the following approximation of Eq. (31) may be used:

$$\eta = \left[\frac{Sh C_b}{\phi[Sh\cosh(\phi) + \phi\sinh(\phi)]}\right]\left[\sinh(\phi) - \frac{\Delta}{8\phi}\cosh(\phi)\right] \tag{32}$$

Eq. (32) was derived using the Taylor series and the perturbation method, it is applicable only for exceedingly small optical thickness. Table 1 shows how the results of Eq. (31) compare with those of Eq. (32). The two solutions are comparable with a very small root mean square error (RMSE = 0.2571).

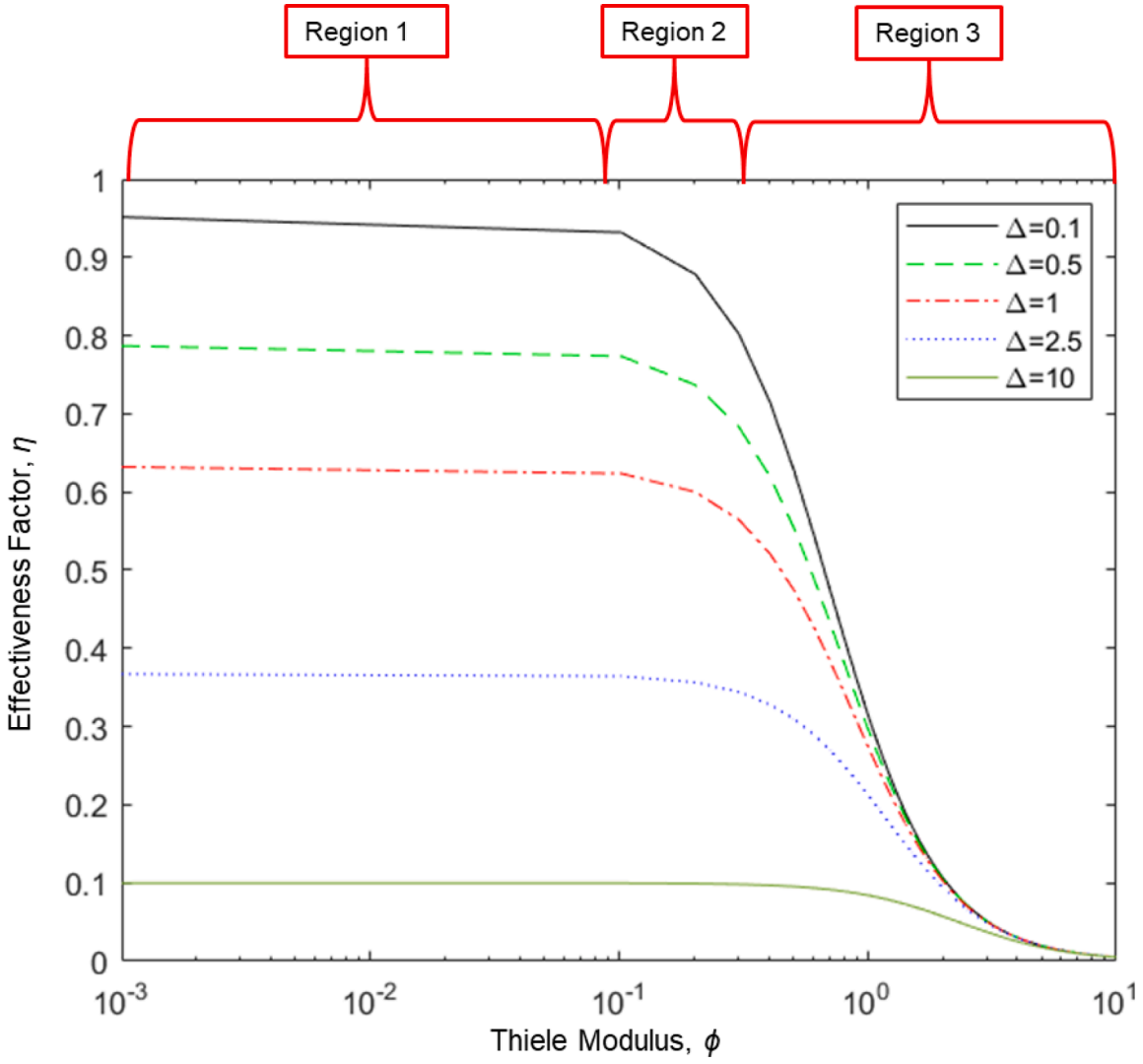

Fig. 3. Effectiveness factor vs Thiele Modulus at different values of the optical thickness (Sh = 0.55).

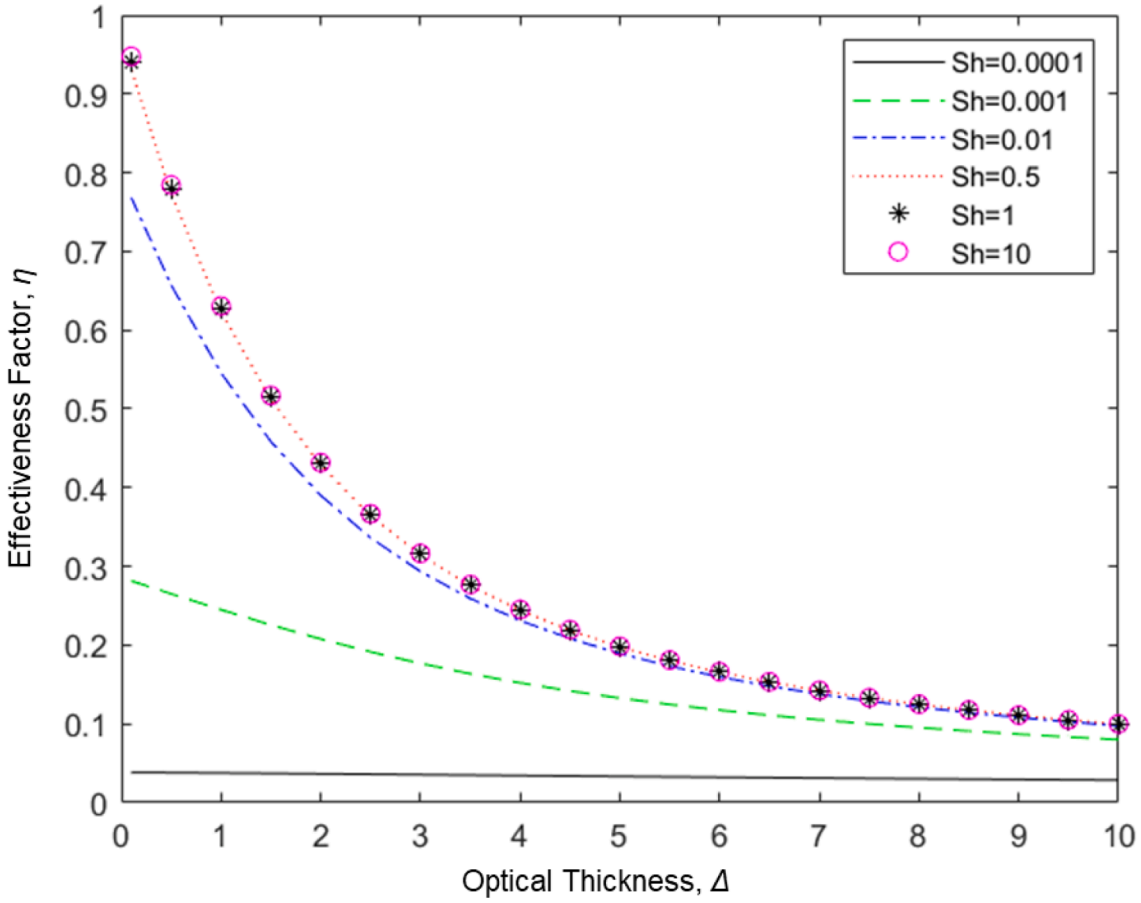

Fig. 4. Effect of Sherwood number on effectiveness factor for $\phi = 0.1$.

3. Results and discussion

3.1. Effect of design parameters on the effectiveness factor

The developed model in Eq. (28) can produce the three operating regions similar to the conventional reactors not utilizing photons as shown in Fig. 3. In region 1 ($\phi < 0.1$) there is minimal internal diffusion resistance, and the process is reaction rate controlled at the catalyst surface, in region 2 ($0.1 < \phi < 1$) the process is limited by the reaction rate, and region 3 ($\phi > 1$) is where internal diffusion resistance is very high.

It is also shown in Fig. 3 that the effectiveness factor decreases with an increase in optical thickness. The optical thickness is one of the most important and complex design parameters of photocatalytic reactors. It is the distance that the photons must travel to be absorbed by the catalyst coating. In Fig. 4 the sensitivity of the effectiveness factor on the optical thickness seems to level off at low Sherwood numbers meaning that the low effectiveness factors are attributed to the external mass transfer limitations.

These effects of the external mass transfer resistance can be seen in Fig. 5 by evaluating the effect of the Sherwood number on the three regions described in Fig. 3. The Sherwood number lumps together the effect of the external mass transfer resistances in the ratio of the convection rate to the diffusion rate. Region 1 as described in Fig. 3 exists in Fig. 5 only at high values of Sherwood number starting from the cut-off value. At low Sherwood numbers this region shifts towards lower ranges of Thiele Modulus, and the free internal diffusion region becomes smaller. The rate of diffusion is high when the Sherwood number is low, but the rate of convection is low. Thus, in this region, the limitation is low transport of the bulk substrate which adversely affects the internal diffusion due to insufficient substrate available. With regards to regions 2 and 3, the effectiveness factor decreases rapidly with an increase in the Thiele Modulus as the Sherwood number is decreased. There is little distinction between these two regions also due to the limited transport of the bulk substrate. In general, the external mass transfer limitations become significant at low Sherwood numbers, due to convective mass transport limitations. Looking at the graphs of $Sh = 0.1$ and $Sh = 0.01$ in Fig. 5, the rapid decrease of the effectiveness factor starts at $\phi = 0.1$ as the Sherwood number is decreased. This is the transition point from which the different controlling mechanisms can be described. Table 2 gives a summary of the possible mechanisms controlling the reaction rate of the photocatalyst layer.

It is also possible that the optical thickness plays a role in the decreased effectiveness factor as it is expected that the photocatalyst surface area becomes less illuminated as the optical thickness is increased. This may lead to fewer photons being absorbed such that only a small area of the catalyst may be activated to initiate the photocatalytic reaction. Thus, further investigations are required to determine the significance of the influence of the two parameters, the Sherwood number, and the optical thickness.

3.2. Model comparison

The calculations of the current model give exact values when compared to the analytical solution of Visan et al., [15] as well as the numerical solution of Edwards et al., [14]. This is illustrated in Table 3 for different values of the optical thickness. Thiele modulus of 0.05 is used in the calculations for comparison since the data from Edwards et al., [14] are reported at this value. The exact values are obtained starting from a cut-off Sherwood value of 0.55, beyond which the present model converges to the other models.

As can be seen in Table 3, the current model deviates from Visan

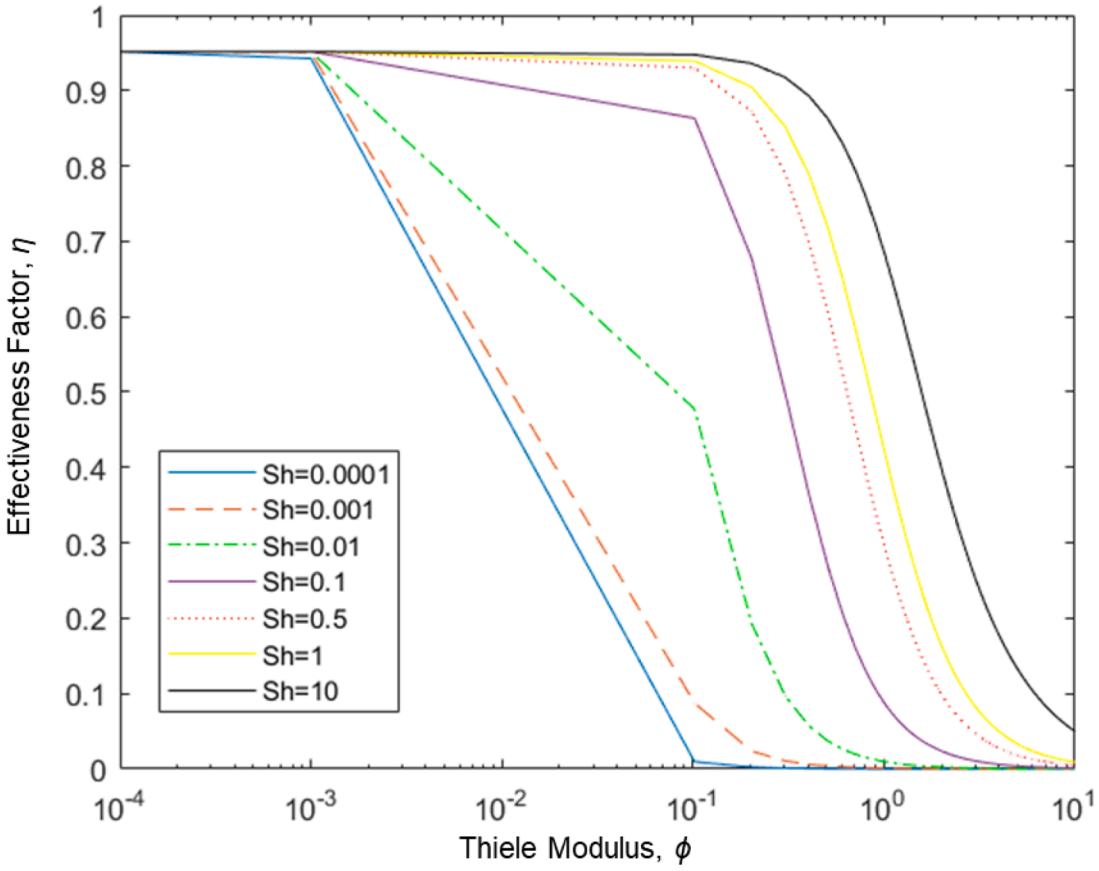

Fig. 5. The effect of the Sherwood number on the effectiveness factor for $\Delta = 0.1$.

Table 2
Controlling mechanisms for photocatalyst layer reaction rate.

Sherwood Number	Thiele Modulus	Controlling Mechanism
$Sh < 0.1$	$\phi < Sh$	Reaction
	$Sh < \phi < 0.1$	External mass transfer
	$0.1 < \phi$	External mass transfer and internal diffusion
$0.1 < Sh$	$\phi < 0.1$	Reaction
	$0.1 < \phi < Sh$	Internal diffusion
	$Sh < \phi$	Internal diffusion and external mass transfer

Table 3
Comparison of the current model with other models ($\varnothing = 0.05$).

	Effectiveness Factor				
			Current Model		
Optical Thickness	Visan	Edwards	Sh = 0.55	Sh = 0.01	Sh = 0.001
0.1	0.94989	–	0.94680	0.76826	0.28156
1	0.63086	0.6319	0.63007	0.54566	0.24494
3	0.31570	0.3167	0.31625	0.29346	0.17675
5	0.19765	–	0.19846	0.18924	0.13272
7	0.14173	0.1427	0.14263	0.13781	0.10519
10	0.09899	0.1	0.09995	0.09756	0.07999

et al., [15] and Edwards et al., [14] for low values of the Sherwood number where external mass transfer limitations are expected because these models only account for internal diffusion resistances. A closer model can be obtained from Rawlings & Ekerdt, [21] and was developed based on the Robin boundary condition for first order reaction in a spherical catalyst. The calculations of this model compare well with the current model at low Sherwood numbers in Table 4. The model in Rawlings & Ekerdt, [21] is for conventional reactors not utilizing photons, hence its applicability to the current model is limited to operations at low optical thickness. The closely comparable values of the effectiveness factor in Table 4 provide confidence in the model presented in this article.

Table 4
Comparison of the current model for low Sh ($\phi = 0.05$, $\Delta = 0.1$).

Sh	Rawlings & Ekerdt, [21]	Current Model
0.55	0.99399	0.94680
0.01	0.79904	0.76826
0.001	0.28560	0.28156

4. Conclusions

An analytical solution for the differential mass balance equation that accounts for the limitations of the external mass transfer is developed in this study for reactions following the first order kinetics. The model calculations compare well with the models found in the literature at the Sherwood number cut-off point of 0.55 and beyond. It has been shown that the external mass transfer limitations cannot be neglected at low values of the Sherwood number. Therefore, the Sherwood number is one of the important design parameters to be included in the models for evaluating the effectiveness factor. The model has been evaluated only for higher Sherwood numbers concerning photocatalytic reactors, however, it compared well with a similar model for conventional reactors at low Sherwood numbers. It will be further evaluated experimentally in photocatalytic reactors using ethylene as the model

pollutant to validate it for Sherwood numbers below the cut-off value. There is confidence in the model since it converges to literature models under Dirichlet boundary condition and can approximate a similar model for convectional reactors at low Sherwood numbers when the optical thickness is low. The model will be applied to reactor design equations for continuous stirred tank reactors (CSTR) and plug flow reactors (PFR) to enable scaling up.

Funding information

The authors would like to acknowledge the National Research Foundation for financial support of the study.

Declaration of Competing Interest

The authors declare that they have no known competing financial interests or personal relationships that could have appeared to influence the work reported in this paper.

Data availability

No data was used for the research described in the article.

References

[1] G.A. Nayik, K. Muzaffar, Developments in Packaging of fresh fruits-shelf life perspective: A review, American Journal of Food Science and Nutrition Research 1 (2014) 34–39. http://www.openscienceonline.com/journal/fsnr.
[2] D. Martínez-Romero, G. Bailén, M. Serrano, F. Guillén, J.M. Valverde, P. Zapata, S. Castillo, D. Valero, Tools to maintain postharvest fruit and vegetable quality through the inhibition of ethylene action: a review, Crit. Rev. Food Sci. Nutr. 47 (2007) 543–560.
[3] A Basso, R. de Fátima Peralta Muniz Moreira, H.J. José, Effect of operational conditions on photocatalytic ethylene degradation applied to control tomato ripening, J. Photochem. Photobiol. A: Chem. 367 (2018) 294–301.
[4] M.L.V. de Chiara, S. Pal, A. Licciulli, M.L. Amodio, G. Colelli, Photocatalytic degradation of ethylene on mesoporous TiO_2/SiO_2 nanocomposites: effects on the ripening of mature green tomatoes, Biosyst. Eng. 132 (2015) 61–70.
[5] M.L.V. de Chiara, L. Spremulli, A. Licciulli, M.L. Amodio, G. Colelli, Design and optimization of fluidized bed photoreactor for ethylene reduction within cold storage room for fruits and vegetables using TiO_2-based materials, Acta Hortic. 1194 (2018) 623–629.
[6] C. Maneerat, Y. Hayata, Efficiency of TiO_2 photocatalytic reaction on delay of fruit ripening and removal of off-flavors from the fruit storage atmosphere, Transactions of the ASABE 49 (2006) 833–837.
[7] T. Nishizawa, M. Takeda, H. Murayama, U. Matsushima, Effects of TiO_2 photocatalytic oxidation in the room atmosphere and the quality of tomato fruit during storage under a closed system, Acta Hortic. 804 (2008) 309–314.
[8] N. Pathak, O.J. Caleb, C. Rauh, P.V. Mahajan, Efficacy of photocatalysis and photolysis systems for the removal of ethylene under different storage conditions, Postharvest Biol. Technol. 147 (2019) 68–77.
[9] R.E. Stroe, L.A. Rosendahl, Kinetic study of the photocatalytic oxidation of ethylene over TiO_2 thin films, IOP Conference Series: Mater. Sci. Eng. 628 (2019).
[10] D. Chen, F. Li, A.K. Ray, Effect of mass transfer and catalyst layer thickness on photocatalytic reaction, AIChE J. 46 (2000) 1034–1045.
[11] F. Parrino, V. Loddo, V. Augugliaro, G. Camera-Roda, G. Palmisano, L. Palmisano, S. Yurdakal, Heterogeneous photocatalysis: guidelines on experimental setup, catalyst characterization, interpretation, and assessment of reactivity, Catal. Rev. - Sci. Eng. 61 (2019) 163–213.
[12] H.S. Fogler, Elements of Chemical Reaction Engineering, Sixth edition., Pearson Education, 2020.
[13] G. Camera-Roda, F. Santarelli, Optimization of the thickness of a photocatalytic film on the basis of the effectiveness factor, Catal. Today 129 (2007) 161–168.
[14] M.E. Edwards, C.M. Villa, C.G. Hill, T.W. Chapman, Effectiveness factors for photocatalytic reactions occurring in planar membranes, Ind. Eng. Chem. Res. 35 (1996) 712–720.
[15] A. Visan, D. Rafieian, W. Ogieglo, R.G.H. Lammertink, Modeling intrinsic kinetics in immobilized photocatalytic microreactors, Appl. Catal. B: Environ. 150–151 (2014) 93–100.
[16] C.G. Hill, T.W. Root. Introduction to Chemical Engineering Kinetics and Reactor Design, Second Edition, John Wiley & Sons, Hoboken, New Jersey, 2014.
[17] O. Levenspiel. Chemical Reaction Engineering, Third edition, John Wiley & Sons, 1999.
[18] M.F.J. Dijkstra, H.J. Panneman, J.G.M. Winkelman, A.A.C.M. Beenackers, J. J. Kelly, Modeling the photocatalytic degradation of formic acid in a reactor with immobilized catalyst, Chem. Eng. Sci. 57 (2002) 4895–4907.
[19] M. Krivec, A. Pohar, G. Dra, Hydrodynamics, mass transfer, and photocatalytic phenol selective oxidation reaction kinetics in a fixed TiO_2, Microreactor. 61 (2015).
[20] M.K. Murshed, A.Y. Dursun, G. Dursun, Application of response surface methodology on photocatalytic degradation of Astrazon orange G dye by ZnO photocatalyst: internal mass transfer effects, Chem. Eng. Res. Design 188 (2022) 27–38.
[21] J.B. Rawlings, J.G. Ekerdt, Chemical Reactor Analysis and Design Fundamentals, Nob Hill Publishing, 2002.
[22] S. Yamazaki, S. Tanaka, H. Tsukamoto, Kinetic studies of oxidation of ethylene over a TiO_2 photocatalyst, J. Photochem. Photobiol. A: Chem. 121 (1999) 55–61.
[23] J. Votruba, J. Sinkule, V. Hlaváček, J. Skřivánek, Heat and mass transfer in monolithic honeycomb catalysts-I, Chem. Eng. Sci. 30 (1975) 117–123.
[24] M. Malayeri, C.S. Lee, F. Haghighat, L. Klimes, Modeling of gas-phase heterogeneous photocatalytic oxidation reactor in the presence of mass transfer limitation and axial dispersion, Chem. Eng. J. 386 (2020).